Biomass Conversion and Biorefinery
https://doi.org/10.1007/s13399-023-04969-1

ORIGINAL ARTICLE

Reaction microkinetic model of xylose dehydration to furfural over beta zeolite catalyst

Emilija Rakić[1] · Andrii Kostyniuk[1] · Nikola Nikačević[2] · Blaž Likozar[1,3,4,5]

Received: 24 July 2023 / Revised: 25 September 2023 / Accepted: 3 October 2023

Abstract
In recent decades, there has been a growing interest in bio-refineries as a crucial element in transitioning to a low-carbon economy. One specific aspect of this interest is the conversion of carbohydrates into separate platform chemicals, such as furfural (FUR), which play a significant functional role in various daily life processes. This research paper focuses on investigating the use of a H-beta catalyst with $SiO_2/Al_2O_3 = 28$ for producing furfural from xylose in water. Various conditions, such as temperature and initial solution concentration, are studied to determine their effect on FUR yield. The highest FUR yield (40 mol.%) is obtained when FUR is the only product species. We also report that about 90% yield from reaction with fresh catalyst can be achieved after catalyst regeneration. The activation energies for the reaction on the catalyst surface are found to be in the range of 38–75 kJ/mol. A mathematical kinetic model with three irreversible steps is derived to estimate the reaction sequence at 160, 180, and 200 °C. The model takes into account mechanisms such as adsorption, desorption, and transport (internal or external). Our results suggest that the H-beta catalyst shows high activity toward FUR yield and could be a promising alternative for mass-scale production of the latter.

Keywords Xylose · Furfural · Dehydration · Reaction · Microkinetic model

1 Introduction

The extensive utilization of fossil fuels in recent times has led to a continuous crisis in the market, climate change, and substantial pollution [1]. To tackle this problem, the production of biofuels derived from cellulose and hemicellulose obtained from biomass waste has emerged as a promising alternative to conventional fuels [2, 3]. The conversion of lignocellulosic materials into fuels and chemicals necessitates the efficient utilization of the C5 sugars found in hemicellulose and the C6 sugars present in cellulose [4]. Furfural (FUR) and 5-hydroxymethylfurfural (HMF) are highly regarded as versatile platform molecules derived from this sugars playing a crucial role in facilitating the transition away from fossil-based industries [5, 6]. In the context of evaluating solvent toxicity, water is recognized as the most environmentally friendly and least toxic choice. However, the implementation of aqueous systems often requires the use of mineral acids [7]. The use of H_2SO_4 [8] and HCl [9], in particular, continues to be the preferred approach for biofuel production. However, these acids are not suitable due to their corrosive nature, high pressure, and temperature requirements and hazardous working conditions [10]. Additionally, the reaction between furfural and xylose can result in the formation of insoluble resinous compounds, which can affect the selectivity of the product and reaction yields [11, 12].

Three different reaction networks are proposed; the first possible reaction network shown in Fig. 1 is a direct reaction of xylose dehydration to furfural without intermediates. Possible byproducts from xylose and furfural decomposition, condensation, and furfural resinification are proposed by Karinen et al. [13]. Such a reaction network has been

✉ Andrii Kostyniuk
andrii.kostyniuk@ki.si

1 Department of Catalysis and Chemical Reaction Engineering, National Institute of Chemistry, Hajdrihova 19, 1001 Ljubljana, Slovenia

2 Faculty of Technology and Metallurgy, University of Belgrade, Belgrade 11120, Serbia

3 Pulp and Paper Institute, 1000 Ljubljana, Slovenia

4 Faculty of Polymer Technology, 2380, Slovenj Gradec, Slovenia

5 Faculty of Chemistry and Chemical Technology, University of Ljubljana, 1001 Ljubljana, Slovenia

Published online: 18 October 2023

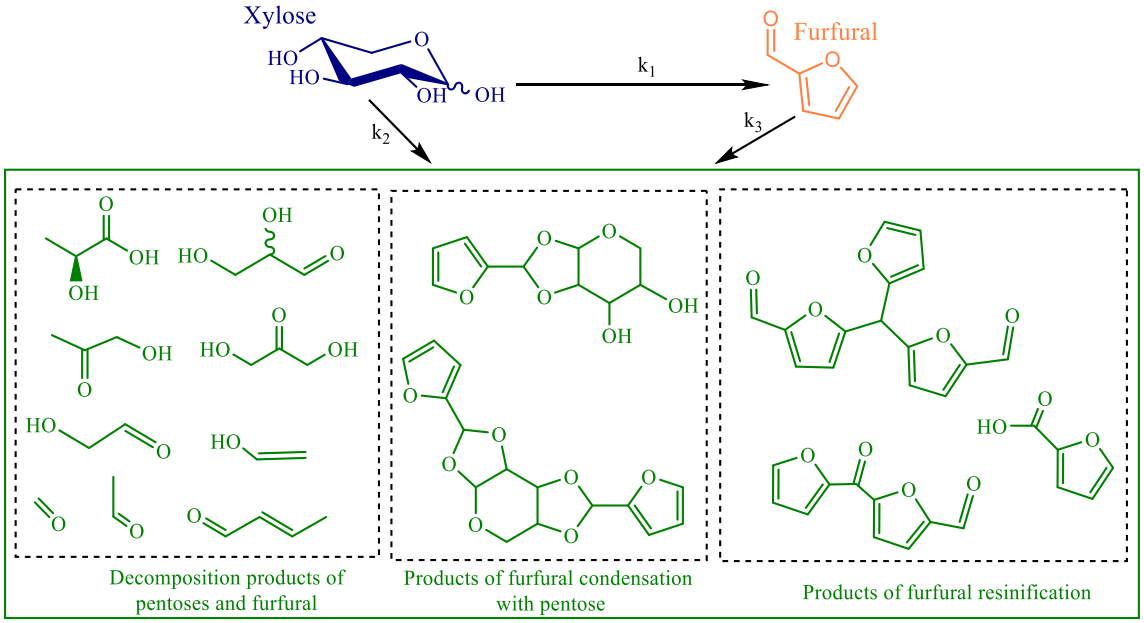

Fig. 1 The reaction pathway with possible byproducts

studied by Aguirrezabal-Telleria et al. [14–17], Chantterjee et al. [18, 19], Fang et al. [20], Peng et al. [21], and Erashova et al. [22, 23] and Job et al. [24]. The first two papers [14, 15] refer to the study of kinetics in the presence of ion-exchange resin Amberlyst 70 in an aqueous medium. Fang et al. [20] referred to this model as a pseudo-homogeneous model consisting of three elementary irreversible steps and found good agreement with experimental data. This model is suitable for cases where no xylose isomers are detected in the reaction mixture. Wang et al. [25] also applied it to the preparation of furfural from sugarcane bagasse in the presence of an acid-acetone-water system. All authors record the occurrence of insoluble oligomers [14–22, 26]. This reaction network is used in this paper.

The second possible reaction network shown in Fig. 2 is more complex than the first, because there is a step involving

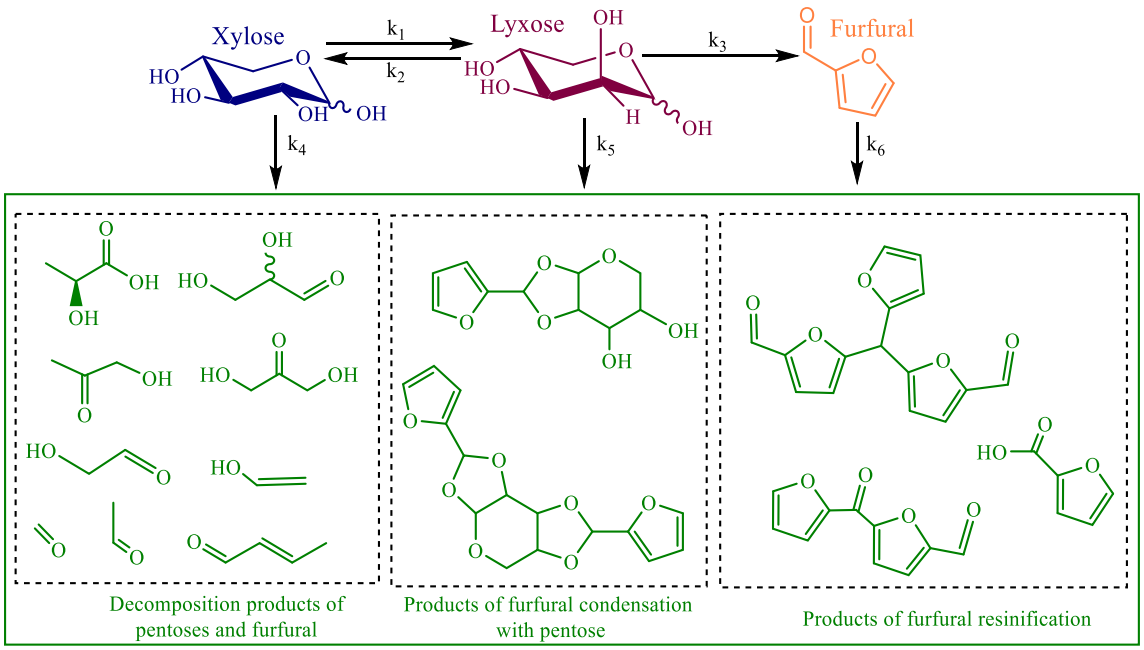

Fig. 2 The second possible reaction pathway with possible byproducts

the isomerization of the xylose to xylulose or lyxose, and this isomer is further dehydrogenated to furfural.

This model differs from the first model in that it involves two more steps of xylose isomerization and decomposition of the xylose isomers into byproducts. The model is suitable for experiments at lower temperatures around 140 °C, where it is possible to detect xylose isomers. Such models have been used by Ferreira et al. [27], O'Neil et al. [28], and Garcia-Sanco et al. [29, 30]. This model agrees well with the experiments but gives lower values for the activation energy than the previous one [13, 27, 31–34].

The third, and most complex model, is presented in Fig. 3, it is derived for alcoholic media and also includes concentrations of alkyl xyloside, which is an intermediate in this reaction. This model assumes an additional reaction between alcohol and xylose, forming insoluble oligomers [35].

In this study, we examined four distinct reaction parameters. Firstly, we investigated the impact of mixing rate to determine the presence of any external resistance to mass transfer. The reactions were carried out at different temperatures to evaluate whether higher temperatures enhance xylose conversion or primarily promote the decomposition of the desired product. Moreover, we explored varying quantities of catalyst, corresponding to different numbers of active sites, and compared these to reactions conducted without a catalyst. Additionally, we modified the initial concentration of xylose to observe its influence on furfural yield in the reaction.

To assess the presence of internal resistance to mass transfer, we calculated relevant parameters. Notably, previous studies commonly assumed the absence of internal mass transfer resistance due to the catalyst's pore size. However, to the best of our knowledge, such calculations have not been performed before for H-beta zeolite. Furthermore, we determined the value of the external mass transfer constant to establish whether the transfer from the liquid phase to the catalyst surface acted as the rate-limiting step in the reaction.

For a more accurate description and potentially scaling up the process, we derived kinetic model parameters. It is worth noting that the model was initially formulated and applied to a homogeneous reaction, which sets our study apart from previous research.

2 Experimental section

2.1 Materials

All reagents, standards, catalysts, and gases were from commercial suppliers and used as supplied. Xylose (99%, Sigma Aldrich, St. Louis, MO, USA) and H-beta zeolite with $SiO_2/Al_2O_3 = 28$ (Tosoh Corporation) were used as the main reactant and catalyst in this reaction, and nitrogen (5.0, Messer,

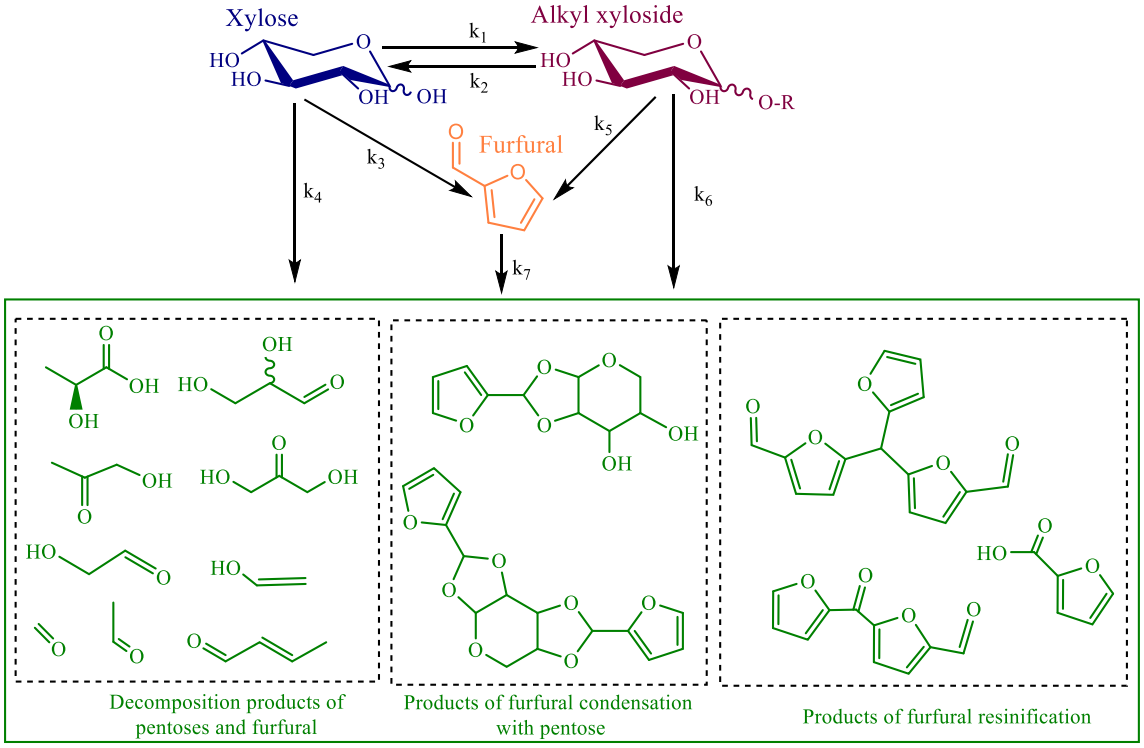

Fig. 3 The third possible reaction pathway with possible byproducts

Gumpoldskirchen, Austria) was used for inert atmosphere and to purge the gas mixture in the reactor before and after the experiments.

Xylose (same as for the reaction), furfural (99%, Sigma-Aldrich, St Louis, MO, USA), lyxose (99%, Sigma Aldrich, St. Louis, MO, USA), glucose (99%, Millipore, Burlington, MS, USA), xylitol (99%, Sigma Aldrich, MO, USA), acetic acid (100%, Sigma Aldrich, MO, USA), levulinic acid (97%, Sigma Aldrich, MO, USA), glycerol (98%, Pharmachem, Slovenia), and 5-hydroxymethylfurfural (99%, Sigma-Aldrich, St Louis, MO, USA) were used for the external calibration.

2.2 Experimental procedure

The reaction was carried out in a system of six parallel batch three-phase reactors manufactured by Amar Equipment Pvt. Ltd. with a volume of 250 mL, maximum operating pressure of 200 bar, and a temperature of 350 °C. The stainless-steel cylindrical reactor vessels are equipped with a Rushton turbine impeller which was magnetically driven. The reaction mixture was prepared by measuring the mass of xylose to obtain the desired concentration in 120 mL of solvent. First, the xylose was weighed and dissolved in a solvent, namely, demineralized water, and then a catalyst was added at the desired mass ratio. The physicochemical properties of the H-beta zeolite catalyst have been shown in Fig. S4. The first experiment was carried out at a temperature of 200 °C, and the nitrogen pressure was 5 bar to achieve an inert atmosphere in the reactor, catalyst mass 1800 µg, and initial xylose concentration 0.1 M. The reaction time was 6 h. Liquid samples were collected directly from the reactor system during the reaction through the equipped sampling tubes. The samples were filtered using cellulose acetate filters (CROMAFIL CA Xtra 20/13) for aqueous or polar samples. The various conditions of all performed experiments are listed in Table S1. For the regeneration test, the spent catalyst from Experiment 3 (Table S1) was filtered from the reaction mixture, dried, and regenerated in air at 600 °C for 6 h. After regeneration, the catalyst was measured and the reaction was performed under the same conditions.

2.3 Catalyst characterization

The structural characteristics of H-beta zeolites were determined by various methods and are listed in Table S2. In each case, the data given in the table were determined in the following manner. The Si and Al contents are a determinant according to inductively coupled plasma optical emission spectroscopy (ICP-OES) using a PerkinElmer Optima 8000. The Brunauer-Emmett-Teller (BET) method was used to determine the surface area using a Micromeritics ASAP 2020 equipment. By using the t-plot method, the total volume of micropores and mesopores was determined. The average pore diameter (PD) was determined using the Barrett, Joyner, and Halenda (BJH) method, while the average crystallite size was determined using X-ray diffraction (XRD) analysis on PANalytical XpertPro instrument using CuKa1 radiation (1.5406 Å) in the range of 2 thetas from 4 to 90° with increments of 0.034°. The surface morphology of the H-beta zeolite was investigated by scanning electron microscopy (SEM) analysis on an FE-SEM SUPRA 35-F (Carl Zeiss) electronic microscope. Acid properties of the H-beta zeolite are shown in Table 1 and analyzed by temperature-programmed desorption of ammonia (NH_3-TPD) using a Micromeritics Autochem 2920 II apparatus equipped with a Pfeiffer Vacuum Thermostar quadrupole mass spectrometer and pyridine adsorption diffuse-reflection infrared spectroscopy (Pyridine-DRIFTS) using a Frontier IR spectrometer (Perkin Elmer) equipped with an MCT detector, DiffusIR® accessory from Pike Scientific [36, 37].

2.4 Product analysis

The reaction mixture was analyzed by HPLC with a Rezex RHM Monosaccharide H+ column using an RI detector to determine sugars and a UV-vis detector to determine furfural and possible byproducts. The observed wavelengths on the UV-vis detector were 210, 254, 270, and 280 nm. The method used was developed by NREL (National Renewable Energy Laboratory) [38]. No byproducts were detected apart from xylose and the desired furfural product. The expected byproducts, including lyxose, glucose, fructose, xylitol, succinic acid, lactic acid, formic acid, acetic acid, levulinic acid, ethyl alcohol, hydroxymethylfurfural, and glycerol,

Table 1 Acid properties of the H-beta zeolite

Acid site density by NH_3-TPD ($mmol_{NH3}/g_{cat}$)				Diversity of acid sites by pyridine-DRIFTS (%)		
Total	Weak[a]	Strong[b]	Strong/Weak	BAS	LAS	BAS/LAS ratio
1.01	0.45	0.57	1.2	54.9	45.1	1.2

[a]—determined at average temperature T = 202.9 °C

[b]—determined at average temperature T = 348.7 °C

BAS—Brönsted acid sites

LAS—Lewis acid sites

were assessed using appropriate standards. Chromatograms depicting the profiles of xylose and furfural can be found in the supplementary data (Fig. S1. and Fig. S2.). Following qualitative and quantitative analyses of the products, the furfural yield and xylose conversion were determined. As furfural is the only product detected with HPLC analysis, we presented results as yield of furfural. The equations for calculating yield and conversion are provided below.

$$\text{Yield, mol\%} = \frac{\text{Real yield}}{\text{Theoretical yield}} \times 100 = \frac{C_{\text{FUR,t}}}{C_{\text{XYL,0}}} \times 100 \tag{1}$$

$$\text{Conversion, mol\%} = \frac{C_{\text{XYL,0}} - C_{\text{XYL,t}}}{C_{\text{XYL,0}}} \times 100 \tag{2}$$

where $C_{\text{XYL,0}}$ is the initial concentration of xylose stoichiometrically calculated; $C_{\text{XYL,t}}$ is the concentration of xylose at time t; and $C_{\text{FUR,t}}$ is the concentration of furfural at time t. The identification and characterization of the degradation product were carried out utilizing size exclusion chromatography (SEC), as depicted in Fig. S3.

3 Microkinetic model

A kinetic model was derived from the assumed reaction network (Fig. 1). The model describes a two-phase liquid-solid system and includes the adsorption and desorption of all components to the catalyst surface, homogeneous reaction in the liquid phase, and the reaction on the catalyst surface (Fig. S5).

The model consists of a set of differential equations for components' material balances, which include the reaction rates, under the following assumptions:

- Based on blank reactions (without the catalyst), a high product concentration was observed in the reaction mixture. At temperatures of 200 and 180 °C, the yield is higher for uncatalyzed reaction because the catalyst accelerates the decomposition of the product. This phenomenon has been studied in the literature as the conversion of xylose in high-temperature water (HTW) [39–41]. Therefore, the reaction in the liquid phase (homogenous) is included in the model.
- Kinetic parameters, reaction rates, and activation energies were determined by conducting reactions in the absence of catalyst in the liquid phase at temperatures of 160, 180, and 200 °C (Fig. S6). These parameters were subsequently incorporated into a system of equations and integrated into the model to accurately determine the reaction parameters on the catalyst surface.
- The reactions on the catalyst surface take place at acidic active sites. Their amount was determined by the NH_3-TPD method.
- Vacant sites are considered equivalent and independent of the total coverage.
- Only one organic molecule can be adsorbed on the one catalyst active site at a time.
- Because of the similarity in structure of the molecules, all adsorption and desorption constants are considered equivalent for all components in the reaction.
- It is important to avoid considering adsorption and desorption as separate phenomena since they are interconnected and constantly balanced. The partitioning of reaction rates between adsorption and desorption in a model is the focus, as the ratio between them determines the surface coverage. Both adsorption and desorption processes are faster than the reactions themselves, leading to the establishment of equilibrium before surface reactions commence. The adsorption/desorption steps were not identified as the rate-determining step in the model.
- Coke formation on the surface of the catalyst, decomposition of the product, and formation of oligomers due to high temperatures have been noted in the literature [42]. The mass of decomposition products and oligomers calculated by the model is labeled as "REST" and given in units of moles per liter in furfural molar equilibrium, as they are assumed to be formed from xylose and furfural and proved by SEC analysis.

The rates of adsorption (r_j^{ads}), desorption (r_j^{des}), surface reaction rate (r_i^{surf}) and homogeneous reaction rate (r_i^{H}) are shown in Eqs. (3)–(6). The adsorption rate of each component j depends on the adsorption rate (k_j^{ads}) constant, its concentration in the liquid phase (C_j^{L}), and the concentration of vacant sites (Θ_{VS}). The desorption rate of each compound j depends on the desorption rate constant (k_j^{des}) and coverage of j adsorbed on active sites (θ_j). The surface reaction rate of each reaction i depends on the surface reaction constant (k_i^{surf}) and the fraction of the corresponding reactant adsorbed on active sites (θ_j). The homogeneous reaction rate of each reaction i depends on the homogeneous reaction rate constant (k_j^{H}) and the concentration in the liquid phase of the reactant involved in the reaction (C_j^{L}).

$$r_j^{ads} = k_j^{ads} \bullet C_J^{L} \bullet \theta_{VS} \tag{3}$$

$$r_j^{des} = k_j^{des} \bullet \theta_j \tag{4}$$

$$r_i^{surf} = k_i^{surf} \bullet \theta_j \tag{5}$$

$$r_i^H = k_i^H \bullet C_J^L \tag{6}$$

During the reaction, the temperature and pressure in the system are measured. During the start-up, the reaction mixture is heated until the desired temperature is reached. This temperature change until the constant value has been also considered in the model. The desorption and adsorption constants are considered to be independent of temperature, while the rate constants are calculated using the Arrhenius law:

$$k_i^{surf}(T_2) = k_i^{surf}(T_1) \times \exp\left(\frac{Ea_i}{R}\left(\frac{1}{T_1} - \frac{1}{T_2}\right)\right) \tag{7}$$

The concentration of components in the liquid phase is given by the mass balance (Eq. (8)), where V is the total volume of the liquid phase while n_{ts} is the total number of active sites on the catalyst surface.

$$\frac{dC_J^L}{dt} = r_j^{ads} + r_j^{des}\frac{n_{ts}}{V} + \sum_i^I \pm r_i^H \tag{8}$$

The coverage of the active sites has been calculated from the expression shown in Eq. (9):

$$\frac{d\theta_j}{dt} = r_j^{ads}\frac{V}{n_{ts}} - r_j^{des} + \sum_i^I \pm r_j^{surf} \tag{9}$$

Vacant site coverage was calculated from Eq. (10)

$$\frac{d\theta_{VS}}{dt} = -\sum_j^J r_j^{ads}\frac{V}{n_{ts}} + \sum_j^J r_j^{des} + \sum_i^I \pm r_i^{surf} \tag{10}$$

The adsorption and desorption constants were determined by an iterative procedure by solving a system of differential equations (S13–S19) for the range of values of the constants from 10^{-10} to 10^{10} and comparing them with the experimental points. It was found that the fixed value of $k_{ads} = 10\ min^{-1}$ and the dependence of the constants $k_{des} = 100 * k_{ads}$ agree well with the experiment. These values are the same for all compounds and are considered independent of temperature.

4 Results and discussion

4.1 Results at 200 °C

Experimental results at 200 °C with an H-beta/xylose mass ratio of 1:1 (Fig. 4A) demonstrate that furfural attains maximum yield after a 120-min time interval, coinciding with the absence of xylose. From the second hour until the end of the experiment, the furfural concentration only decreases. The maximum yield achieved in this reaction is 31.5%, which diminishes to 14.5% at the conclusion of the reaction. Conversely, when the catalyst mass is halved (Fig. 4B), a higher furfural yield is observed. The maximum yield of 42% is attained after 90 min of reaction. In comparison to the 1:1 mass ratio, the furfural concentration exhibits faster growth in this reaction, while the xylose concentration profile remains relatively unchanged. The final furfural yield reaches 18.9%, indicating accelerated decomposition and oligomerization of furfural and xylose facilitated by the catalyst. Examination of the uncatalyzed reaction (Fig. S6) reveals a higher yield at 200 °C without the presence of a catalyst than in the presence of the catalyst in the reaction mixture, suggesting that our catalyst exhibits activity but not selectivity towards furfural for this reaction. The concentration values obtained from the model (lines in Fig. 4A) predict a slightly higher furfural yield and follow the decreasing trend of its concentration. When the catalyst mass is halved (Fig. 4B), the model predicts a slightly lower furfural concentration. Based on visual observation of the reaction mixture, the color of the catalyst, high-resolution scanning electron microscopy (HRSEM) images, and size-exclusion chromatography (SEC) analysis, and the reaction of furfural with the same reaction conditions on 200 °C (Fig. S7.), it can be inferred that furfural forms oligomers that adhere

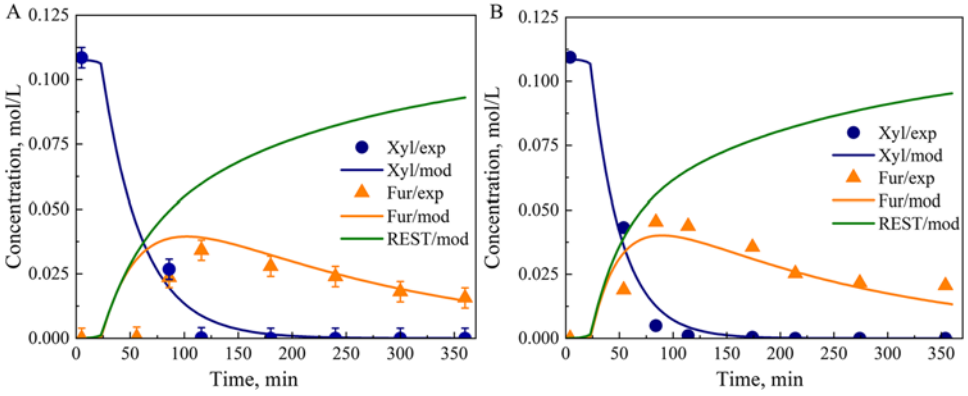

Fig. 4 Model (lines) and experimental (points) data at 200 °C. Reaction conditions: $P_{N2} = 5$ bar, stirring speed = 1000 rpm, initial xylose concentration $C_{Xyl} = 0.1$ mol/L, mass ratio of H-beta/xylose = 1:1 (**A**) and 1:2 (**B**). Experimental error was determined to be ± 5%

to the reactor wall due to the high temperature and remains on the catalyst and filters. In terms of mechanistic elucidation, it was determined that Brønsted and Lewis acid catalytic activities play distinct roles. Brønsted acidity was found to enhance the direct dehydration of xylose, while the presence of Lewis acidity was observed to facilitate the isomerization of xylose through a mechanistic pathway [43]. The influence of temperature on the zeolite-catalyzed reaction has been studied in the temperature range of 140–220 °C by O'Neil et al. [28]. It was observed that the product was rapidly degraded to solid-insoluble compounds. At higher temperatures, furfural was very unstable and degraded faster, especially at 200–220 °C [28]. The catalyst promotes side reactions and degradation as well as the formation of oligomers. Studies show that the reaction pathway for dehydration of xylose in water can be altered by manipulating the temperature without the catalyst [6, 39–41]. In the study by Jing et al. [39], the main product of xylose was furfural, whose maximum yield of the molecular fraction was 50%, the reaction mixture was darker due to the presence of furfural, and there were no insoluble compounds. The 50% yield of furfural in HTV (high-temperature water) was attributed to high Kv (ionic water product) [39]. At high temperatures, above 160 °C, water can self-ionize and form the H_3O^+ ion, which acts as a Brönsted acid and catalyzes the conversion of xylose [14]. The reason for the maximum 50% yield is attributed to the condensation reaction between xylose and the product during an extended presence in water [39]. When utilizing birch hydrolysate as the pentose source, the optimized conditions for a two-phase dehydration reaction, with the presence of cyclopentyl methyl ether (CPME) in a volume ratio of 1:1, resulted in a maximum FUR yield of 68% and a xylose conversion of 96% after 90 min. This was achieved in an auto-catalyzed reaction at a temperature of 190 °C [2]. Auto-catalyzed reactions with furfural yield better results when water is combined with an organic solvent such as water/MBIK systems [44]. The higher solubility of furfural in organic solvents reduces the possibility of further reaction, degradation, and oligomerization. Gomez Milan et al. [2] achieved a yield of 68% at 190 °C in the presence of cyclopentyl methyl ether and water. Lin et al. [45] achieved a yield of 81.6% using DMSO/water without additional catalyst, and Guo et al. [46] achieved a yield of 84.3% at 200 °C with a water:DMSO ratio of 1:1.

4.2 Results at 180 °C

The investigation into lower reaction temperatures was pursued in order to mitigate furfural degradation within the reaction mixture. At a reaction temperature of 180 °C, the furfural yield is slightly lower compared to 200 °C. The highest yield observed in this scenario is 33.9% for the reaction with a xylose-to-catalyst mass ratio of 1:1, and 39.8% for the reaction with half the catalyst mass. The peak yield is achieved within the initial 3 h of the reaction, coinciding with near-complete xylose conversion. Towards the end of the reaction, the concentration of furfural decreases due to decomposition and oligomer formation, albeit at a slower rate than at 200 °C. As shown in Fig. 5B, the reduced catalyst weight yields a slightly higher output (39.8%) in comparison to the xylose-to-catalyst mass ratio of 1:1 (33.9%) shown in Fig. 5A. In these reactions (Fig. 5), the peak yield is attained later than in the 200 °C reactions (Fig. 4). This delay is attributed to the combined effects of a higher catalyst mass and elevated temperature, which accelerate xylose conversion and furfural degradation. A higher yield is also observed in the reactions without catalysts, consistent with the studies on xylose conversion in the absence of catalysts, where this phenomenon is observed at temperatures above 180 °C. Regarding the model, there are certain discrepancies with the experimental results. The model predicts a faster rise in furfural concentration. When the catalyst and xylose masses are equal, the model aligns better with the experimental data. However, when the catalyst mass is lower, the model anticipates lower furfural concentrations and slightly higher and faster xylose conversion.

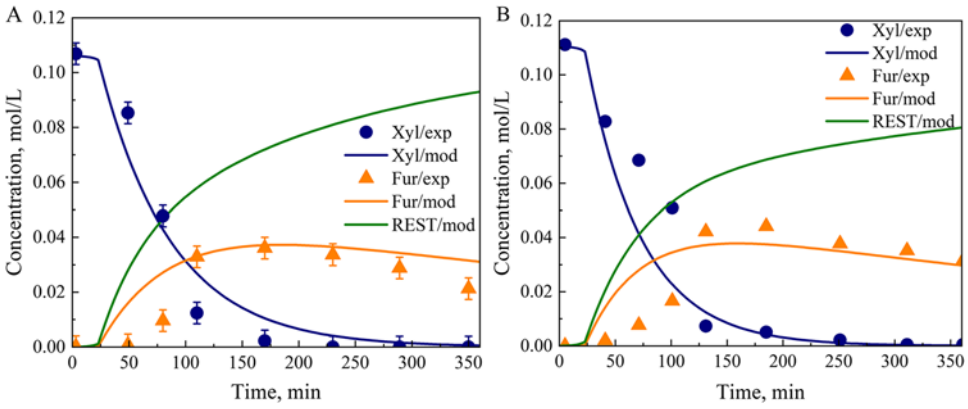

Fig. 5 Model and experimental data at 180 °C. Reaction conditions: P_{N2} = 5 bar, stirring speed = 1000 rpm, initial xylose concentration C_{Xyl} = 0.1 mol/L, mass ratio of H-beta/xylose = 1:1 (**A**) and 1:2 (**B**). Experimental error was determined to be ± 5%

4.3 Results at 160 °C

4.3.1 Effect of the catalyst loading

To investigate the influence of the catalyst at a temperature of 160 °C, various cases were examined. The mass ratios of xylose to catalyst ranging from 1:1 to 1:4 were explored, as well as the case with twice as many catalysts as xylose. The results, depicted in Fig. 6, revealed that at this temperature, the furfural concentration did not decrease as significantly as at higher temperatures, indicating greater stability of furfural. The highest yield was observed when the catalyst was present in the same amount as xylose in the reaction mixture (Fig. 6A). As the catalyst mass decreased, the furfural yield declined from 32.2 (Fig. 6A) to 26.2% (Fig. 6B), while the xylose concentration was higher in the reaction with half the catalyst mass. The influence of the catalyst on xylose conversion appeared to be less critical compared to temperature. The study also investigated the effect of doubling the catalyst mass (Fig. 6C), which resulted in the lowest yield of 18.8%.

This confirmed the hypothesis that an increased catalyst extent accelerates the decomposition and oligomerization of the desired product. The xylose concentration profile in Fig. 6A remained similar in Fig. 6C, indicating that the catalyst's influence on xylose conversion is not as significant as the temperature's influence. Experiments with a reduced amount of catalyst (Figs. 6D and 6E) demonstrated a slight decrease in yield when the catalyst amount was decreased at a temperature of 160 °C. The xylose concentration profile in Fig. 6B, 6D, and 6E exhibited almost identical trends.

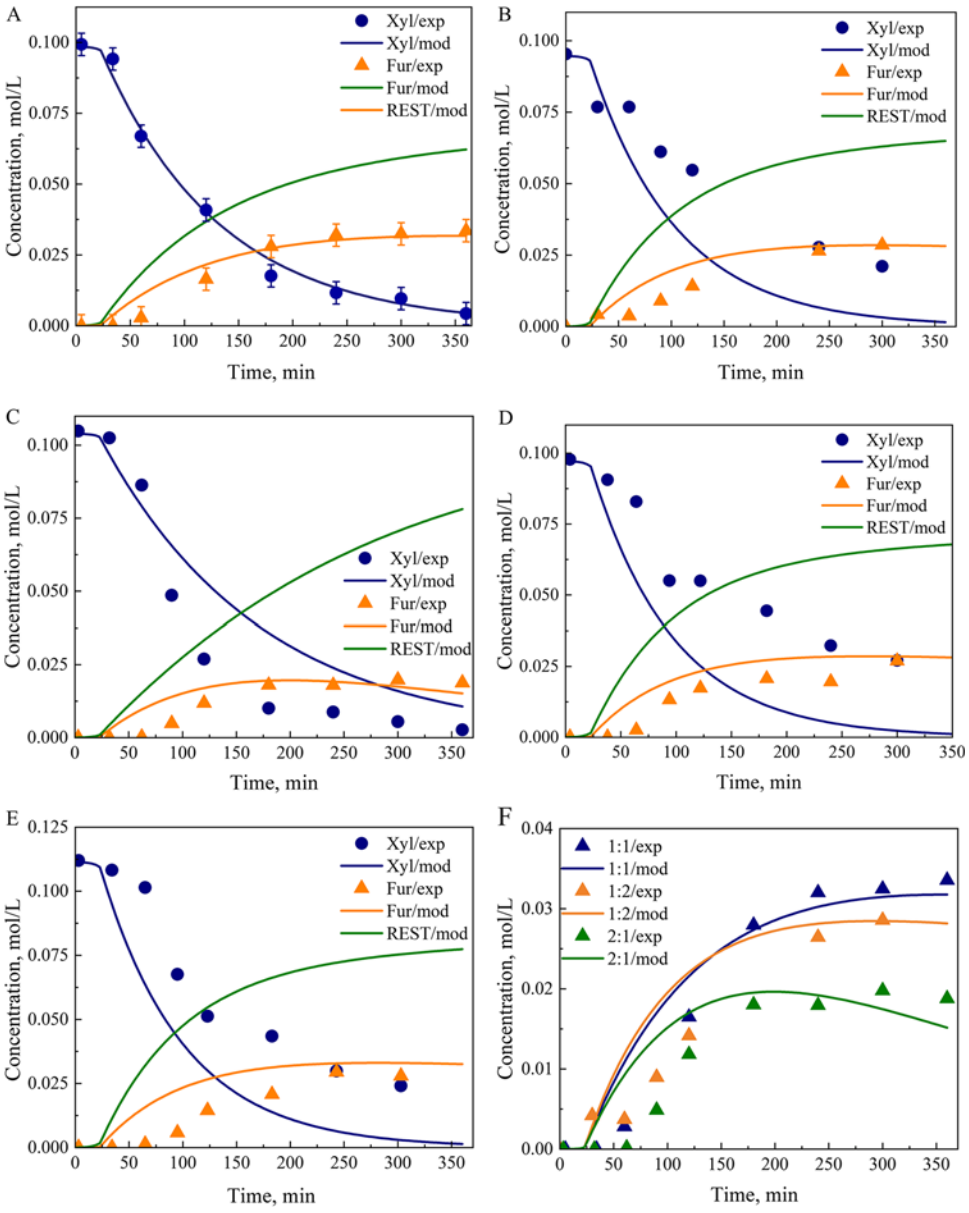

Fig. 6 Model and experimental data at 160 °C. Reaction conditions: P_{N2} = 5 bar, stirring speed = 1000 rpm, initial xylose concentration C_{Xyl} = 0.1 mol/L, mass ratio of H-beta/xylose = 1:1 (**A**), 1:2 (**B**), 2:1 (**C**), 1:3 (**D**), 1:4 (**E**), and furfural concentration for all experiments (**F**). Experimental error was determined to be ± 5%

Fig. 6F provides an overview of all furfural concentration profiles, highlighting that the optimal reaction conditions correspond to a mass ratio of 1:1. The model calculations demonstrated good agreement with the experimental trends (Fig. 6), indicating an overall reliable description of the system. However, discrepancies emerged in cases where the catalyst mass was reduced, resulting in the model predicting lower xylose concentrations and higher conversions (Fig. 6B, 6D, and 6E).

For zeolites in water, used for furfural production, the ratios of 1:1, 1:3, 1:4, and 3:2 are common [28, 33, 47, 48]. Such ratios allow the concentration of furfural in the reaction mixture to increase during the whole reaction time, which is consistent with our experiments. Kim et al. [33] utilized H-beta zeolite with $SiO_2/Al_2O_3 = 25$ at 140 °C with a maximum furfural yield of 12% in a time interval of 6 h. To study H-beta zeolite, Ferreira et al. [27] used it in water at 170 °C, which gave a yield of 30% after 8 h of reaction.

4.3.2 Effect of xylose concentration

In order to investigate and understand the influence of the initial concentration of xylose on the yield of furfural in the reaction, a series of experiments was conducted. The initial concentration of xylose was systematically varied within the range of 0.05 to 0.2 mol/L. The objective was to determine how different concentrations of xylose affected the production of furfural. It was observed that the reaction with the lowest initial concentration of xylose resulted in the highest yield of furfural. However, this particular reaction took the longest time to reach the maximum concentration of furfural in the reaction mixture. On the other hand, as the concentration of xylose in the solution increased, the furfural yield gradually decreased. This suggests a clear correlation between the initial xylose concentration and the final furfural yield. Throughout all the experiments, unreacted xylose was found to be present in the solution until the end of the reaction, indicating that the conversion of xylose to furfural was not complete. This observation highlights the need for further optimization and improvement in the reaction conditions to enhance the conversion efficiency. The experimental results demonstrated that the furfural yields at the end of the reaction varied depending on the initial xylose concentration. Specifically, the yield was 21.4% for a concentration of 0.2 mol/L (Fig. 7A), 22.7% for a concentration of 0.175 mol/L (Fig. 7B), 32.2% for a concentration of 0.1 mol/L (Fig. 7C), 34.7% for a concentration of 0.075 mol/L (Fig. 7D), and 36.9% for a concentration of 0.05 mol/L (Fig. 7E). We experimented with higher concentrations, specifically 5 wt% and 10 wt%, as initial concentrations of xylose, which resulted in yields of 20% and 18%, respectively. These findings offer compelling evidence that the initial xylose concentration has a direct impact on the ultimate furfural yield (Fig. 7F).

Comparing the experimental data with the model predictions, it was found that the model generally agreed with the experimental results. For higher initial concentrations of xylose (Fig. 7A, B), the model accurately predicted higher concentrations of both xylose and furfural. In the case of the intermediate concentration (Fig. 7C), the model demonstrated excellent agreement with the experimental data. However, for lower initial concentrations of xylose (Fig. 7D, E), the model underestimated the concentrations of xylose and furfural, indicating a limitation in its predictive capabilities under those specific conditions.

In the literature, the known initial values of xylose concentration in the reactor are in the range of 0.01–0.5 M [27, 28, 33, 39, 41, 47, 49]. The results of previous research indicate that a near linear relationship can be observed between increasing initial xylose concentration and the resulting decrease in furfural concentration. This phenomenon is explained by the fact that an excess of xylose in the solution leads to the formation of byproducts [41]. In cases where other solvents are used in combination with water, such as γ-valerolactone, the furfural yield is independent of the xylose concentration [50].

4.4 Regenerated catalyst

The experiments show that fresh and regenerated catalysts achieve almost identical values for xylose conversion under the same conditions (Fig. 8B). For fresh catalyst, the conversion was 92.2% and for regenerated it was 93.3%. The yield of furfural in the first reaction with fresh catalyst was 32.2% and with regenerated catalyst 30.0%, which is about 90% of the yield obtained with fresh catalyst (Fig. 8A).

Aho et al. [42] investigated the regeneration of H-beta zeolite. After the experiment, the spent zeolite separated by sieving, was regenerated in a calcination furnace at 450 °C for only 2 h. After regeneration, the number of active sites and acidity were measured. It was found that the regenerated H-beta zeolite recovered 90% of the original active surfaces; therefore, the regeneration was considered successful [42]. In their second paper [51], they also regenerated this catalyst, but the residence time in the furnace was not sufficient to turn the catalyst white (completely regenerated) but showed darker spots where char residues remained. It took only 20 min at 500 °C to restore 96.1% of zeolite active sites, although the coke remained on the catalyst, this did not appear to affect the activity of the catalyst [51].

4.5 Mass transfer calculations and experiments

For the compounds that are transferred from the liquid phase to the external surface of the catalyst, the mass transfer constant

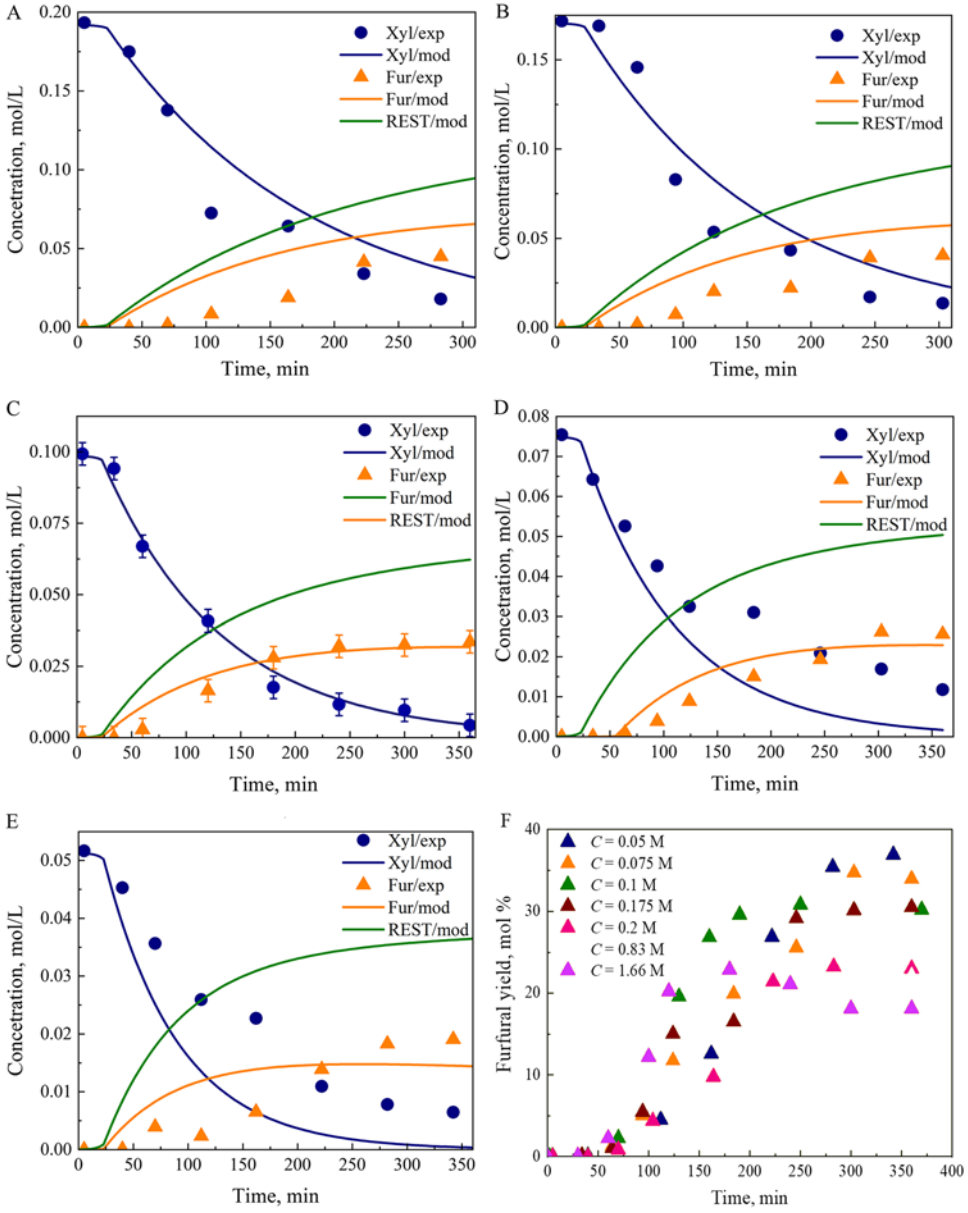

Fig. 7 Model and experimental data at 160 °C. Reaction conditions: P_{N2} = 5 bar, stirring speed = 1000 rpm, the mass ratio of H-beta/xylose = 1:1, with different xylose concentrations (C_{Xyl}) as follows 0.2 M (**A**), 0.175 M (**B**), 0.1 M (**C**), 0.075 M (**D**), 0.05 M (**E**), and furfural yield for all experiments (**F**). Experimental error was determined to be ± 5%

was calculated from the Frösling correlation [52] given in Eq. (11). Meaning of symbols in Eqs. (11) to (14) are as follows: Sherwood number, Sh; Reynolds number, Re; Schmidt number, Sc; fluid velocity, U; fluid density, ρ; catalyst diameter, dp; fluid viscosity, μ; kinematic viscosity of fluid, ν; and diffusion coefficient, D_{ab}. The diffusion coefficient D_{ab} is calculated from Eq. (15) proposed by Mogi et al. [53]. Adjustable constants α and β for xylose are 2.057×10^{-5} and −1.016, and temperature T was set at 453.15 K [53].

$$Sh = 2 + 0.6\mathrm{Re}^{1/2}Sc^{1/3} \tag{11}$$

$$\mathrm{Re} = \frac{U\rho d_p}{\mu} \tag{12}$$

$$Sc = \frac{\nu}{D_{ab}} \tag{13}$$

$$k_l = \frac{ShD_{ab}}{d_p} \tag{14}$$

$$D_{ab} = \alpha\mu^{\beta}T \tag{15}$$

Mass transfer constant is calculated as $k_l = 7.7$ m/s. To better describe this phenomenon, experiments were conducted at different stirring speeds (Table S1), and the results are shown in Fig. 9. It is noticeable that the results of the experiments at 600 and 800 rpm almost coincide. Almost identical yields of furfural were obtained at these stirring speeds, which is

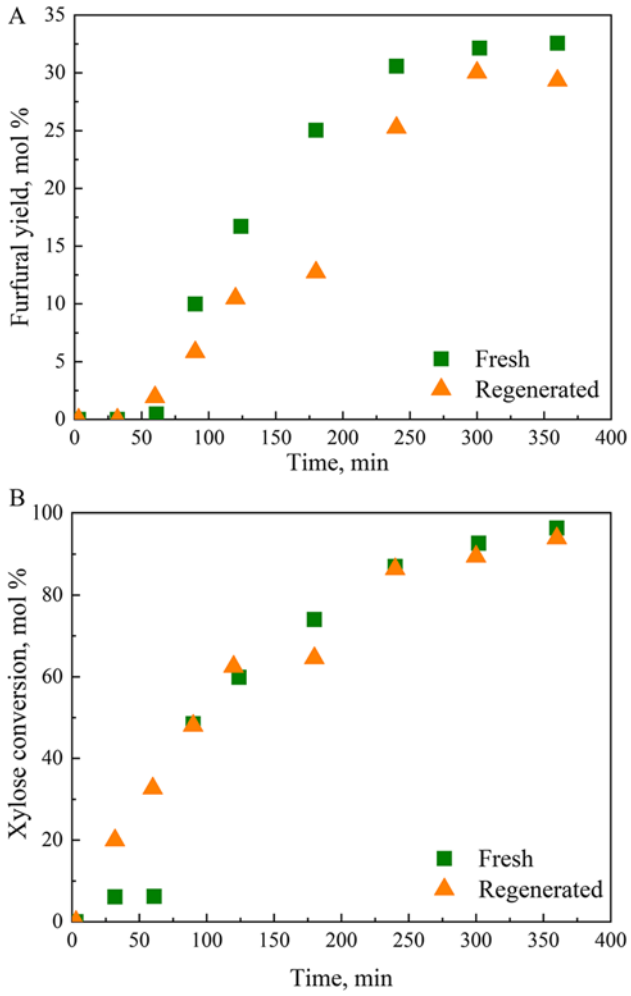

Fig. 8 Experimental data at 160 °C. Reaction conditions: P_{N2} = 5 bar, stirring speed = 1000 rpm, mass ratio of H-beta/xylose = 1:1, initial xylose concentration C_{Xyl} = 0.1 M for the fresh and regenerated catalysts with furfural yield (**A**) and xylose conversion (**B**). Experimental error was determined to be ± 5%

also the case for xylose conversion. At 1000 rpm, slightly higher values were obtained for the furfural concentration in the reaction mixture. Difference can be the consequence of the experimental error. At this stirring speed (1000 rpm), the conversion of xylose reaches the maximum value faster, a difference of several percent in two samples during the reaction, and at the end of the reaction, there is almost no significant difference in the last samples at all speeds.

In the literature, such tests have been performed with zeolites in the range of 400–1200 rpm [21, 27, 28, 35]. It was found that above the value of 600 rpm, the resistance to external mass transfer is negligible for microporous zeolites. Nzediegwu et al. [54] found that the optimum stirring speed for the preparation of HMF and furfural from C6 and C5 sugars is 600 rpm. They carried out the experiments and obtained only 3% higher yield at a stirring speed of 800 rpm. The resistance to internal mass transfer was found to be negligible when the size of catalyst particles determined by SEM is in micrometers [28]. Ferreira et al. noted that increasing the stirring speed from 400 to 700 rpm accelerated the reaction but performed all experiments at 1000 rpm to make sure there was no internal or external resistance to mass transfer [27]. Soukup-Carne et al. [55] noted in their review article on microkinetic models for furan production from carbohydrates that most studies have generally been conducted under stirring conditions where there is no restriction on external mass transfer. Mass transfer constant k_l calculated in this work is fast enough not to influence the chemical reaction.

To prove that and to show how much the rate of the chemical reaction is slowed by diffusion into catalyst pores, an effectiveness factor was also calculated.

$$\varepsilon = \frac{1}{M_t}\left(\frac{1}{tahn3M_t} - \frac{1}{3M_t}\right) \tag{16}$$

$$M_t = \frac{L}{3}\sqrt{\frac{k}{D_{ef}}} \tag{17}$$

$$D_{ef} = \frac{7.4 \bullet 10^{-8}\left(\phi M_B\right)^{1/2} T}{\mu_B V_A^{0,6}} \tag{18}$$

The effectiveness factor ε is a function of the Thiele modulus M_t, calculated from Eq. (16); D_{ef}

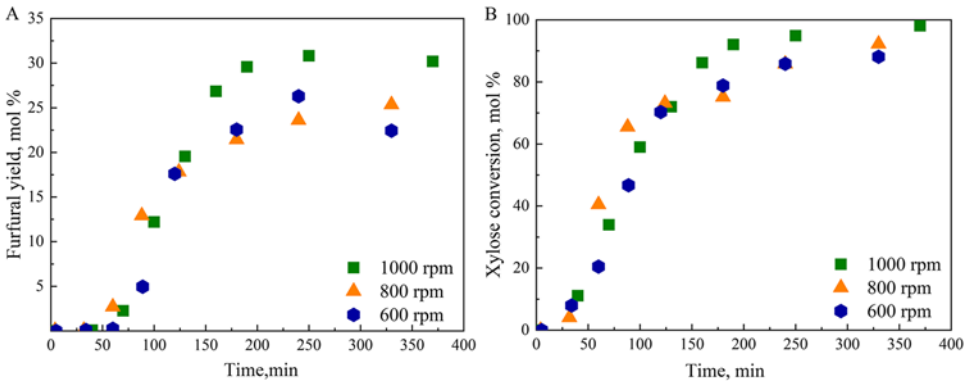

Fig. 9 Furfural yield (**A**) and xylose conversion (**B**) with different stirring speeds. Reaction conditions: P_{N2} = 5 bar, mass ratio of H-beta/xylose = 1:1, initial xylose concentration C_{Xyl} = 0.1 M at 160 °C. Experimental error was determined to be ± 5%

represents the effective diffusivity, and it is calculated from Wilke-Chang correlation (Eq. (16)) [52, 56]. The meaning of the symbols in Eqs. (16)−(18) are as follows: specific length, L, which represents the radius of the catalyst sphere; molecular weight of solvent, M_B; viscosity of the solvent, μ_B; molar volume of xylose at its initial boiling point temperature, V_A; and association factor of a solvent, $\phi = 2.6$ if the solvent is water. The rate constant of the reaction, k, was determined from the experiments, assuming that it is a first order reaction, as stated in almost all sources about the xylose reaction. The molar volume of xylose is calculated from the Cheneo correlation [56].

Given the complex and non-linear nature of the pore structure in zeolites, which includes tortuous pathways and non-uniform shapes, characterizing diffusion on an individual pore basis is impractical. Instead, the effective diffusion coefficient (De) is calculated to represent the average diffusion behavior within porous solids. De serves as an estimation of the overall diffusion process, considering the diverse pathways and irregularities encountered within the zeolite structure. The calculation for D_e is as follows:

$$De = \frac{D_{AB}\epsilon}{\tau} \tag{19}$$

where D_{AB} represents the molecular diffusion coefficient of reactant A in solvent B calculated using the Wilke-Chang correlation, τ is tortuosity, and ϵ is the porosity of the catalyst. For this catalyst, a typical value for tortuosity of 4 and a porosity of 0.3 as a conservative estimate based on literature sources [57–59]. The calculated value of the effectiveness factor is 0.995 which confirms that reaction is not limited by internal diffusion.

4.6 Kinetic modelling results

Table 2 shows the set of kinetic parameters acquired for both homogeneous reactions and reactions occurring on the catalyst surface. The activation energies pertaining to the surface reaction exhibit a range between 38 and 75 kJ/mol. Notably, in the specific case of xylose conversion, the activation energy stands out as the highest among the reactions investigated. This suggests that the reaction of xylose conversion is particularly stimulated at elevated temperatures, emphasizing that the kinetic rate constant for this reaction is highly sensitive to temperature fluctuations. Analyzing the values of the kinetic constants, it becomes apparent that the conversion of xylose to degradation products constitutes the predominant rapid step, owing to its considerably high kinetic rate. On the other hand, with regard to the homogeneous reaction, it is evident that the process of furfural oligomerization is primarily promoted at higher temperatures due to its notable activation energy. The activation energy range for homogeneous reaction is from 24 to 94 kJ/mol. The correlation coefficient for furfural experimental and model results is provided in the supplementary file (Fig. S8).

Homogeneous catalysis has been described in previous studies [39–41]. Jing et al. [39] investigated the reaction kinetics in HTW (high-temperature water) at reaction conditions between 180 and 220 °C. It was found to be an identical reaction pathway and the magnitudes of the obtained constants ($k_1^H = 0.00450$ min^{-1}, $k_2^H = 0.00322$ min^{-1}, $k_3^H = 0.00128$ min^{-1}) are in agreement with those determined in this work, as well as the activation energies, which are between 58 and 140 kJ/mol [39]. Hua et al. [41] estimated the parameter for the xylose conversion step $k^H = 0.00379$ min^{-1}, $E_a = 68$ kJ/mol, which agrees with the parameters k_2^H and E_{a2}^H obtained in this work.

For the surface reactions, Ferreira et al. [27] calculated the values of reaction rate constants for the conversion of xylose and their value ranges from 0.027 to 2.468 h^{-1}. The kinetic model is based on a more complicated reaction network with byproducts. Although nanocrystalline beta zeolite was used, the reaction conditions were different, microreactor and lower temperature, which could be the reason for the discrepancy between the results of this study and our study [27]. Peng et al. [21] calculated activation energies and reaction rate constants for this reaction in the temperature range of 110–140 °C in the presence of heteropolyacids and obtained $k_1$surf = 0.12 min^{-1}, $k_2$surf = 0.002 min^{-1},

Table 2 Kinetic parameters used in the model

i	Reactants	Products	Reaction rate (r_i) [min^{-1}]	Reaction rate constants k_i [min^{-1}]	Activation energy (E_{ai}) [kJ/mol]
Surface reactions					
1	Xyl	Fur	$k_1^{surf}\theta_{xyl}$	$(7.1 \pm 2.2) \times 10^{-1}$	74.8 ± 9.6
2	Fur	DP	$k_2^{surf}\theta_{fur}$	$(1.7 \pm 0.9) \times 10^{-3}$	44.4 ± 3.4
3	Xyl	DP	$k_3^{surf}\theta_{xyl}$	$(9.5 \pm 0.1) \times 10^{-1}$	37.7 ± 10.0
Homogeneous reactions					
1	Xyl	Fur	$k_1^H C_{xyl}$	$(6.5 \pm 0.5) \times 10^{-3}$	47.5 ± 9.9
2	Fur	DP	$k_2^H C_{fur}$	$(4.5 \pm 0.1) \times 10^{-3}$	94.1 ± 12.1
3	Xyl	DP	$k_3^H C_{xyl}$	$(2.2 \pm 0.3) \times 10^{-3}$	24.5 ± 2.6

Xyl xylose, *Fur* furfural, *DP* decomposition products

$k_3$surf = 0.004 min^{-1}, E_{a1} = 85.1 kJ/mol, E_{a2} = 82.0 kJ/mol, E_{a3} = 46.9 kJ/mol which are slightly higher than activation energies obtained in this work. O Niel et al. [28] calculated activation energies in the range of 39.5–131 kJ/mol; these values are almost in the same range as ours. The activation energy calculated by Chatterjee et al. [19] for the conversion of xylose to furfural (E_a = 43 kJ/mol) agrees with E_{a2} for the surface reaction. To resume, the kinetic parameters determined in this work agree well with those previously determined in the literature. In the cases where there are slight discrepancies, the reason may be the use of different reaction conditions or the absence of homogeneous reaction parameters in the model. In their review article, Saucup-Karne et al. stated that kinetic models have been developed to elucidate the furan production process in both monophasic and biphasic operations. These models consider various reaction networks that are potentially involved. Through comprehensive analysis of numerous case studies conducted in both types of operations, it has been observed that the activation energy values are typically up to 110 mol^{-1} [55].

5 Conclusions

In the pursuit of environmentally friendlier furfural production utilizing water as a non-toxic solvent, zeolites have emerged as promising contenders. Zeolite H-beta, in particular, presents a viable alternative to conventional homogeneous catalysts. Our study extensively examined diverse experimental parameters influencing furfural yield within the context of xylose dehydration, all conducted in the presence of water as the solvent. These parameters encompassed temperature, initial xylose concentration, catalyst quantity, stirring rate, and catalyst site regeneration for the H-beta catalyst.

Furthermore, our investigation delved into kinetic modeling to unveil the underlying mechanisms. We determined kinetic parameters for both surface and homogeneous reactions, revealing intriguing insights. Activation energies for surface reactions ranged from 38 to 75 kJ/mol, with xylose conversion exhibiting the highest activation energy. This signifies its sensitivity to temperature fluctuations, underscoring the importance of elevated temperatures in promoting xylose conversion.

The analysis of kinetic constants indicated that the primary rapid step involves the conversion of xylose into degradation products due to its notably high kinetic rate. In contrast, homogeneous reactions, specifically furfural oligomerization, were particularly favored at higher temperatures due to their substantial activation energy, spanning 24 to 94 kJ/mol.

Through alignment of our model's predictions with experimental results, we validated its accuracy for reactions without catalysts and with catalyst/xylose ratios of 1:1 and 1:2 across all utilized reaction temperatures.

Supplementary Information The online version contains supplementary material available at https://doi.org/10.1007/s13399-023-04969-1.

Acknowledgements The authors acknowledge financial support from the EU Framework Programme for Research and Innovation Horizon 2020 under Grant Agreement No. 887226 (BioSPRINT) and from the Slovenian Research Agency (research core funding No. P2-0152, J2-2492, J2-1723, and J7-1816). Also, the authors would like to acknowledge funding from the Slovenian Research Agency (ARRS) and the Science Fund of the Republic of Serbia (SFRS) in the form of a joint bilateral project BI-RS/20-21-002. ARRS is also acknowledged for project funding J1-3020.

Author contributions ER: data curation; formal analysis, investigation, methodology, visualization, roles/writing (original draft), writing (review and editing). AK: supervision, formal analysis, writing—review and editing, software, visualization, validation. NK: writing—review and editing. BL: conceptualization, funding acquisition, project administration, supervision, writing—review and editing.

Data Availability Data will be made available on request.

Declarations

Ethical approval Not applicable

Competing interests The authors declare no competing interests.

References

1. Borges MS, Barbosa RS, Rambo MKD et al (2022) Evaluation of residual biomass produced in Cerrado Tocantinense as potential raw biomass for biorefinery. Biomass Convers Biorefin 12:3055–3066. https://doi.org/10.1007/s13399-020-00892-x
2. Gómez Millán G, Hellsten S, King AWT et al (2019) A comparative study of water-immiscible organic solvents in the production of furfural from xylose and birch hydrolysate. J Ind Eng Chem 72:354–363. https://doi.org/10.1016/j.jiec.2018.12.037
3. Nuchdang S, Thongtus V, Khemkhao M et al (2021) Enhanced production of reducing sugars from paragrass using microwave-assisted alkaline pretreatment. Biomass Convers Biorefin 11:2471–2483. https://doi.org/10.1007/s13399-020-00624-1

4. Luo Y, Li Z, Li X et al (2019) The production of furfural directly from hemicellulose in lignocellulosic biomass: a review. Catal Today 319:14–24. https://doi.org/10.1016/j.cattod.2018.06.042
5. Xu C, Paone E, Rodríguez-Padrón D et al (2020) Recent catalytic routes for the preparation and the upgrading of biomass derived furfural and 5-hydroxymethylfurfural. Chem Soc Rev 49:4273–4306. https://doi.org/10.1039/d0cs00041h
6. Piqueras CM, Cabeza Á, Gallina G et al (2017) Online integrated fractionation-hydrolysis of lignocellulosic biomass using sub- and supercritical water. Chem Eng J 308:110–125. https://doi.org/10.1016/j.cej.2016.09.007
7. Lee CBTL, Wu TY (2021) A review on solvent systems for furfural production from lignocellulosic biomass. Renew Sustain Energy Rev 137:110172. https://doi.org/10.1016/j.rser.2020.110172
8. Danon B, Hongsiri W, van der Aa L, de Jong W (2014) Kinetic study on homogeneously catalyzed xylose dehydration to furfural in the presence of arabinose and glucose. Biomass Bioenergy 66:364–370. https://doi.org/10.1016/j.biombioe.2014.04.007
9. Jaswal A, Singh PP, Mondal T (2022) Furfural – a versatile, biomass-derived platform chemical for the production of renewable chemicals. Green Chem. https://doi.org/10.1039/D1GC03278J
10. Wang J, Wang JH, Yu YM (2021) Effective and safer catalyst KHSO4 for producing furfural: a platform compound. Biomass Convers Biorefin 11:1293–1300. https://doi.org/10.1007/s13399-019-00516-z
11. Slak J, Pomeroy B, Kostyniuk A et al (2022) A review of biorefining process intensification in catalytic conversion reactions, separations and purifications of hydroxymethylfurfural (HMF) and furfural. Chem Eng J 429. https://doi.org/10.1016/j.cej.2021.132325
12. Gómez Millán G, Bangalore Ashok RP, Oinas P et al (2021) Furfural production from xylose and birch hydrolysate liquor in a biphasic system and techno-economic analysis. Biomass Convers Biorefin 11:2095–2106. https://doi.org/10.1007/s13399-020-00702-4
13. Karinen R, Vilonen K, Niemelä M (2011) Biorefining: Heterogeneously catalyzed reactions of carbohydrates for the production of furfural and hydroxymethylfurfural. ChemSusChem 4:1002–1016. https://doi.org/10.1002/cssc.201000375
14. Agirrezabal-Telleria I, García-Sancho C, Maireles-Torres P, Arias PL (2013) Dehydration of xylose to furfural using a Lewis or Brönsted acid catalyst and N2 stripping. Chinese J Catal 34:1402–1406. https://doi.org/10.1016/s1872-2067(12)60599-3
15. Agirrezabal-Telleria I, Larreategui A, Requies J et al (2011) Furfural production from xylose using sulfonic ion-exchange resins (Amberlyst) and simultaneous stripping with nitrogen. Bioresour Technol 102:7478–7485. https://doi.org/10.1016/j.biortech.2011.05.015
16. Agirrezabal-Telleria I, Requies J, Güemez MB, Arias PL (2014) Dehydration of d-xylose to furfural using selective and hydrothermally stable arenesulfonic SBA-15 catalysts. Appl Catal B Environ 145:34–42. https://doi.org/10.1016/j.apcatb.2012.11.010
17. Agirrezabal-Telleria I, Gandarias I, Arias PL (2014) Heterogeneous acid-catalysts for the production of furan-derived compounds (furfural and hydroxymethylfurfural) from renewable carbohydrates: a review. Catal Today 234:42–58. https://doi.org/10.1016/j.cattod.2013.11.027
18. Chatterjee A, Hu X, Lam FLY (2018) A dual acidic hydrothermally stable MOF-composite for upgrading xylose to furfural. Appl Catal A Gen 566:130–139. https://doi.org/10.1016/j.apcata.2018.04.016
19. Chatterjee A, Hu X, Lam FLY (2019) Modified coal fly ash waste as an efficient heterogeneous catalyst for dehydration of xylose to furfural in biphasic medium. Fuel 239:726–736. https://doi.org/10.1016/j.fuel.2018.10.138
20. Fang C, Wu W, Li H et al (2017) Production of bio-based furfural from xylose over a recyclable niobium phosphate (NbOPO3) catalyst. Energy Sources, Part A Recover Util Environ Eff 39:2072–2077. https://doi.org/10.1080/15567036.2017.1402103
21. Peng L, Wang M, Li H et al (2020) tert -Butanol intervention enables chemoselective conversion of xylose to furfuryl alcohol over heteropolyacids. Green Chem 22:5656–5665. https://doi.org/10.1039/d0gc02001j
22. Ershova O, Nieminen K, Sixta H (2017) The role of various chlorides on xylose conversion to furfural: experiments and kinetic modeling. ChemCatChem 9:3031–3040. https://doi.org/10.1002/cctc.201700269
23. Ershova O, Kanervo J, Hellsten S, Sixta H (2015) The role of xylulose as an intermediate in xylose conversion to furfural: insights via experiments and kinetic modelling. RSC Adv 5:66727–66737. https://doi.org/10.1039/c5ra10855a
24. Job AL, Stratton SM, Umhey CE et al (2022) Using artificial neural networks to estimate xylose conversion and furfural yield for autocatalytic dehydration reactions. ACS Sustain Chem Eng 10:177–181. https://doi.org/10.1021/acssuschemeng.1c05413
25. Wang Q, Zhuang X, Wang W et al (2018) Rapid and simultaneous production of furfural and cellulose-rich residue from sugarcane bagasse using a pressurized phosphoric acid-acetone-water system. Chem Eng J 334:698–706. https://doi.org/10.1016/j.cej.2017.10.089
26. Ricciardi L, Verboom W, Lange JP, Huskens J (2022) Production of furans from C5 and C6sugars in the presence of polar organic solvents. Sustain Energy Fuels 6:11–28
27. Ferreira LR, Lima S, Neves P et al (2013) Aqueous phase reactions of pentoses in the presence of nanocrystalline zeolite beta: identification of by-products and kinetic modelling. Chem Eng J 215–216:772–783. https://doi.org/10.1016/j.cej.2012.11.022
28. O'Neil R, Ahmad MN, Vanoye L, Aiouache F (2009) Kinetics of aqueous phase dehydration of xylose into furfural catalyzed by ZSM-5 zeolite. Ind Eng Chem Res 48:4300–4306. https://doi.org/10.1021/ie801599k
29. García-Sancho C, Agirrezabal-Telleria I, Güemez MB, Maireles-Torres P (2014) Dehydration of d-xylose to furfural using different supported niobia catalysts. Appl Catal B Environ 152:1–10. https://doi.org/10.1016/j.apcatb.2014.01.013
30. García-Sancho C, Sádaba I, Moreno-Tost R et al (2013) Dehydration of xylose to furfural over MCM-41-supported niobium-oxide catalysts. ChemSusChem 6:635–642. https://doi.org/10.1002/cssc.201200881
31. Bruce SM, Zong Z, Chatzidimitriou A et al (2016) Small pore zeolite catalysts for furfural synthesis from xylose and switchgrass in a γ-valerolactone/water solvent. J Mol Catal A Chem 422:18–22. https://doi.org/10.1016/j.molcata.2016.02.025
32. Lam E, Majid E, Leung ACW et al (2011) Synthesis of furfural from xylose by heterogeneous and reusable nafion catalysts. ChemSusChem 4:535–541. https://doi.org/10.1002/cssc.201100023
33. Kim SB, You SJ, Kim YT et al (2011) Dehydration of D-xylose into furfural over H-zeolites. Korean J Chem Eng 28:710–716. https://doi.org/10.1007/s11814-010-0417-y
34. Lam E, Chong JH, Majid E et al (2012) Carbocatalytic dehydration of xylose to furfural in water. Carbon N Y 50:1033–1043. https://doi.org/10.1016/j.carbon.2011.10.007
35. Iglesias J, Melero JA, Morales G et al (2016) Dehydration of xylose to furfural in alcohol media in the presence of solid acid catalysts. ChemCatChem 8:2089–2099. https://doi.org/10.1002/cctc.201600292

36. Lašič Jurković D, Kostyniuk A, Likozar B (2022) Mechanisms, reaction micro-kinetics and modelling of hydrocracking of aromatic biomass tar model compounds into benzene, toluene and xylenes (BTX) over H-ZSM-5 catalyst. Chem Eng J 445. https://doi.org/10.1016/j.cej.2022.136898
37. Kostyniuk A, Bajec D, Likozar B (2022) Catalytic hydrocracking reactions of tetralin biomass tar model compound to benzene, toluene and xylenes (BTX) over metal-modified ZSM-5 in ambient pressure reactor. Renew Energy 188:240–255. https://doi.org/10.1016/j.renene.2022.01.090
38. Sluiter A, Hames B, Ruiz R et al (2008) Determination of structural carbohydrates and lignin in biomass: laboratory analytical procedure (LAP). Nat Renew Energy Lab 1617(1):1–6
39. Jing Q, Lu X, Yuan L (2006) Kinetics of non-catalyzed decomposition of xylose in high temperature liquid water. Huaxue Fanying Gongcheng Yu Gongyi/Chemical React Eng Technol 22:472–475. https://doi.org/10.1016/s1004-9541(07)60143-8
40. Aida TM, Shiraishi N, Kubo M et al (2010) Reaction kinetics of d-xylose in sub- and supercritical water. J Supercrit Fluids 55:208–216. https://doi.org/10.1016/j.supflu.2010.08.013
41. Hua DR, Wu YL, Liu YF et al (2016) Preparation of furfural and reaction kinetics of xylose dehydration to furfural in high-temperature water. Pet Sci 13:167–172. https://doi.org/10.1007/s12182-015-0069-y
42. Aho A, Kumar N, Eränen K et al (2007) Catalytic pyrolysis of biomass in a fluidized bed reactor: Influence of the acidity of h-beta zeolite. Process Saf Environ Prot 85:473–480. https://doi.org/10.1205/psep07012
43. Choudhary V, Sandler SI, Vlachos DG (2012) Conversion of xylose to furfural using Lewis and Brønsted acid catalysts in aqueous media. ACS Catal 2:2022–2028. https://doi.org/10.1021/cs300265d
44. Sweygers N, Depuydt DEC, Van Vuure AW et al (2020) Simultaneous production of 5-hydroxymethylfurfural and furfural from bamboo (Phyllostachys nigra "Boryana") in a biphasic reaction system. Chem Eng J 386:123957. https://doi.org/10.1016/j.cej.2019.123957
45. Lin Q, Zhan Q, Li R et al (2021) Solvent effect on xylose-to-furfural reaction in biphasic systems: Combined experiments with theoretical calculations. Green Chem 23:8510–8518. https://doi.org/10.1039/d1gc02812j
46. Guo X, Guo F, Li Y et al (2018) Dehydration of D-xylose into furfural over bimetallic salts of heteropolyacid in DMSO/H2O mixture. Appl Catal A Gen 558:18–25. https://doi.org/10.1016/j.apcata.2018.03.027
47. Antunes MM, Lima S, Fernandes A et al (2012) Aqueous-phase dehydration of xylose to furfural in the presence of MCM-22 and ITQ-2 solid acid catalysts. Appl Catal A Gen 417:243–252. https://doi.org/10.1016/j.apcata.2011.12.046
48. Lima S, Antunes MM, Fernandes A et al (2010) Acid-catalysed conversion of saccharides into furanic aldehydes in the presence of three-dimensional mesoporous Al-TUD-1. Molecules 15:3863–3877. https://doi.org/10.3390/molecules15063863
49. Shi X, Wu Y, Yi H et al (2011) Selective preparation of furfural from xylose over sulfonic acid functionalized mesoporous Sba-15 materials. Energies 4:669–684. https://doi.org/10.3390/en4040669
50. Sener C, Motagamwala AH, Alonso DM, Dumesic JA (2018) Enhanced furfural yields from xylose dehydration in the Γ-valerolactone/water solvent system at elevated temperatures. ChemSusChem 11:2321–2331. https://doi.org/10.1002/cssc.201800730
51. Aho A, Tokarev A, Backman P et al (2011) Catalytic pyrolysis of pine biomass over H-beta zeolite in a dual-fluidized bed reactor: effect of space velocity on the yield and composition of pyrolysis products. Top Catal 54:941–948. https://doi.org/10.1007/s11244-011-9716-8
52. Vicente B, Nori M, Fogler HS (2005) Solutions manual for elements of chemical reaction engineering. Prentice Hall
53. Mogi N, Sugai E, Fuse Y, Funazukuri T (2007) Infinite dilution binary diffusion coefficients for six sugars at 0.1 MPa and temperatures from (273.2 to 353.2) K. J Chem Eng Data 52:40–43. https://doi.org/10.1021/je0601816
54. Nzediegwu E, Pérez-Venegas M, Auclair K, Dumont M-J (2022) Semisynthetic production of hydroxymethylfurfural and furfural: the benefits of an integrated approach. J Environ Chem Eng 10:108515. https://doi.org/10.1016/j.jece.2022.108515
55. Soukup-Carne D, Fan X, Esteban J (2022) An overview and analysis of the thermodynamic and kinetic models used in the production of 5-hydroxymethylfurfural and furfural. Chem Eng J 442:136313. https://doi.org/10.1016/j.cej.2022.136313
56. Poling BE, Prausnitz JM, O'Connell JP (2001) The properties of gases and liquids. McGraw-Hill
57. Mowla O, Kennedy E, Stockenhuber M (2019) Mass transfer and kinetic study on BEA zeolite-catalysed oil hydroesterification. Renew Energy 135:417–425. https://doi.org/10.1016/j.renene.2018.12.012
58. Nelson ML, Romo JE, Wettstein SG, Seymour JD (2021) Impact of xylose on dynamics of water diffusion in mesoporous zeolites measured by nmr. Molecules 26:5518. https://doi.org/10.3390/molecules26185518
59. Baroi C, Mahto S, Niu C, Dalai AK (2014) Biofuel production from green seed canola oil using zeolites. Appl Catal A Gen 469:18–32. https://doi.org/10.1016/j.apcata.2013.09.034